Networks and Heterogeneous Media

NHM, 20(3): 885–902.
DOI: 10.3934/nhm.2025038
Received: 21 May 2025
Revised: 29 June 2025
Accepted: 10 July 2025
Published: 25 July 2025

https://www.aimspress.com/journal/NHM

Research article

Boundary layer flow and heat transfer of viscoelastic fluid embedded in a non-Darcy porous medium with double fractional Maxwell model

Jinhu Zhao*

School of Mathematics and Statistics, Fuyang Normal University, Fuyang 236037, China

* **Correspondence:** Email: jinhuzhao@fynu.edu.cn; Tel: 18298113066.

Abstract: A novel numerical simulation was conducted for boundary layer flow and heat transfer of viscoelastic fluid in a non-Darcy porous medium. The double fractional Maxwell model and generalized Fourier's law were employed in constitutive relation and heat transport, respectively. The strongly coupled and nonlinear fractional governing equations were formulated, which were solved and validated by the finite volume method combined with the fractional $L1$ scheme. The influences of fractional derivative parameters, Darcy number, porosity, and inertial parameter on the transport fields are discussed. Our results demonstrated that the different fractional derivative parameters exhibit opposite influences on velocity/temperature distributions. Moreover, the inertial effects induce velocity profile crossover that marks the transition between viscous and inertial dominance. These findings redefine our understanding of energy transport in complex porous systems.

Keywords: boundary layer flow; non-Darcy porous medium; double fractional Maxwell model; fractional finite volume method

Nomenclature: c_f: geometric factor of the base fluid; *Pr*: Prandtl number; *Da*: Darcy number; *q*: heat flux; *g*: acceleration due to gravity; *Ra*: Rayleigh number; G: shear modulus; *t*: (dimensionless) time; *K*: permeability of the porous matrix; *T*: temperature; k_m: thermal conductivity of the porous medium: *u, v*: (dimensionless) velocity components; *L*: length of the plate; *x, y*: (dimensionless) coordinate; α, β: fractional derivative parameter; γ, η: fractional derivative parameter; α_m: thermal diffusivity; β_T: thermal expansion coefficient; μ: dynamic viscosity; ν_f: kinematic viscosity; θ: dimensionless temperature; ϕ: porosity; ρ_f: density of the base fluid; ρc: heat

capacity; λ_1, λ_2: (dimensionless) relaxation time; τ_{xy}: shear stress component; σ: thermal capacity ratio; ε: shear strain; ζ: shear rate; $\Gamma(\cdot)$: Gamma function; Λ: inertial parameter; *w*: wall condition; *f*: fluid; ∞: ambient condition; *m*: porous medium; *s*: solid matrix

1. Introduction

The investigation of heat transfer in porous media has received continuous attention due to its widespread applications in geothermal processes, reservoir engineering, storage of foodstuffs, chemical reactor engineering [1], etc. For moderate and fast flows, the classical Darcy law is invalid because inertia effects are prevalent. Vafai and Tien [2] analyzed the influence of inertia and solid boundary adequately in porous media. El-Amin [3] investigated the joint effect of solutal diffusivity and thermal dispersion on the heat transfer rate for non-Darcy porous medium. Narayana and Murthy [4] investigated the influence of double stratification on dimensionless heat and mass transfer embedded in non-Darcy porous media. Pal and Mondal [5] discussed the effect of variable viscosity on the MHD convective heat transfer in non-Darcy porous medium. El-Zehairy et al. [6] presented a pore-network model to simulate non-Darcy convection through porous medium.

In recent years, the constitutive relations with fractional derivatives were verified as excellently flexible for viscoelastic dynamics in the characterization of memory effects. Song et al. [7] proposed the fractional viscoelastic Maxwell model to simulate the dynamic moduli of gum. Xu and Chen [8] constructed the fractional differential model to characterize the complex viscoelastic creep characteristics of Hami Melon. The fractional fractal diffusion model was established by Yang et al. [9] to describe the transmission mechanism of gas in heterogeneous coal matrix. Yao [10] presented an adjustable fractional order dashpot that can realize continuous control of dissipation degree between the whole dashpot and Maxwell model. Su et al. [11] clarified the physical connotation behind the fractional-order viscoelastic model by establishing the equivalent viscoelastic correspondence. Wei et al. [12–14] presented stability analysis and error estimation of numerical solutions for time-dependent differential equations, including fractional Black-Scholes option pricing model and fractional sub-diffusion model. Wang et al. made important contributions in other fractional and fractal models [15–17], such as the fractional complex Ginzburg–Landau model, low-pass electrical transmission lines model, and Schrodinger equation with fractal derivatives. Furthermore, the double fractional Maxwell model was found to be more accurate and stable to characterize the constitutive properties of viscoelastic fluids. Tan et al. [18] derived an analytical solution for the unsteady flow of viscoelastic fluid between parallel plates based on the double fractional Maxwell model. Hayat et al. [19] constructed exact analytic solutions for the flows stimulated by periodic oscillations with the double fractional Maxwell model. Yin and Zhu [20] presented the unidirectional oscillating flow of double fractional Maxwell viscoelastic fluid in the infinite extension of the straight pipe. Chen et al. [21] constructed the double fractional Maxwell model to analyze the flow characteristics of viscoelastic fluid in the boundary layer on the surface of a stretched sheet. Yang et al. investigated the boundary layer flow and heat exchange on a stretched plate with thickness variation and simulated the viscoelastic behavior of arterial walls using the double fractional Maxwell model [22, 23].

On the other hand, Caputo and Plastino [24] carried out research showing that the interaction between solid and water molecules leads to the historical dependence of water flow in porous structures. Hence, relevant studies on porous media with fractional derivatives have also been conducted widely in the literature [25]. Zhou and Yang [26] introduced fractional order Darcy's law to describe the non-

Darcy flow phenomena of high and low speed. Zhou et al. [27] modeled the non-Darcy flow and solute migration in porous medium by the improved Caputo fractional derivative. Yang et al. [28] constructed the Swartzendruber model to characterize the nonlinear seepage in porous structures using conformable derivative. Alaimo et al. [29] incorporated the time memory effect into the constitutive equation between flux and pressure in the non-Darcy flow by the Caputo fractional derivative. Wei et al. [30] introduced two Swartzendruber models based on fractional calculus to characterize nonlinear seepage behavior in porous media. Wang developed a new fractal model of the convective-radiative heat transfer equation in porous media [31] and proposed a new fractional exothermic reactions model with constant heat source in porous media [32]. Parmar et al. [33] proposed a fractional order double-diffusion model to analyze the transient nature of fluid flow within a wavy porous cavity. Haider [34] analyzed heat and mass transfer in Sutterby fluid within porous media by integrating Caputo's fractional derivative. Nevertheless, little research has been conducted to discuss the flow and heat transfer phenomena driven by thermal buoyancy in non-Darcy porous media with a double fractional Maxwell model.

In view of this, we introduce a novel dual-fractional constitutive framework, combining the double fractional Maxwell model with an extended generalized Fourier's Law, to investigate non-Darcy convective flow and heat transfer in porous media under constant heat flux conditions. The interrelated governing equations are constructed with strongly nonlinear fractional convection terms. The finite volume method is developed to discretize the fractional boundary layer equations combined with the $L1$ scheme. Exact solutions of special terms are conducted to validate the derived numerical solutions. Finally, the influence mechanism of major parameters on fluid velocity distribution and the temperature gradient is discussed, such as fractional derivative parameters, Darcy number, porosity, and the inertial parameter.

2. Mathematical formulation

Unsteady, incompressible, laminar natural convection embedded in homogeneous, isotropic non-Darcy porous media over a vertical plate is discussed. The x-axis extends along the surface of the plate, and the y-axis is orthogonal to the surface. At the initial moment, the fluid is stationary with homogeneous boundary conditions. Constant ambient temperature outside and from the plate is T_∞, while the wall heat flux q is maintained as a constant for $t>0$. It is assumed that the solid matrix and the fluid reach thermodynamic equilibrium in the local spatial domain. Except for the density changes with temperature, the rest of the physical properties of the fluid remain unchanged. The governing equations of momentum and energy equations can be derived as follows:

$$\frac{1}{\phi}\frac{\partial u}{\partial t}+\frac{1}{\phi^2}\left[\frac{\partial}{\partial x}\left(uu\right)+\frac{\partial}{\partial y}\left(vu\right)\right]=\frac{1}{\phi\rho_f}\frac{\partial \tau_{xy}}{\partial y}+g\beta_T\left(T-T_\infty\right)-\frac{\nu_f}{K}u-\frac{c_f}{\sqrt{K}}u^2, \tag{1}$$

$$\left(\rho c\right)_m\frac{\partial T}{\partial t}+\left(\rho c\right)_f\left[\frac{\partial}{\partial x}\left(uT\right)+\frac{\partial}{\partial y}\left(vT\right)\right]=-\frac{\partial q}{\partial y}, \tag{2}$$

where u and v are the velocity components, ϕ is the porosity, ρ_f is the density of the base fluid, τ_{xy} is the shear stress component, g is the acceleration due to gravity, β_T is the thermal expansion coefficient, T is the temperature, ν_f is the kinematic viscosity, K is the permeability of the porous

matrix, c_F is the geometric factor of the base fluid, $(\rho c)_m = \phi(\rho c)_f + (1-\phi)(\rho c)_s$, $(\rho c)_f$, and $(\rho c)_s$ are the heat capacities of the porous media, base fluid, and solid matrix, respectively, and q is the heat flux.

The fractional constitutive relation with a double Maxwell model is an advanced viscoelastic model that exhibits two distinct relaxation times corresponding to different molecular or microstructural relaxation processes [35]. This model is particularly useful for capturing viscoelastic responses observed in polymers, biological tissues, and other soft materials, which is employed as:

$$\tau_{xy} + \lambda_1^{\alpha} \frac{\partial^{\alpha} \tau_{xy}}{\partial t^{\alpha}} = G\lambda_1^{\beta} \frac{\partial^{\beta} \varepsilon}{\partial t^{\beta}}, \quad 0 < \alpha \le \beta < 1, \tag{3}$$

where ε is the shear strain, G is the shear modulus, $\lambda_1 = \mu / G$ is the relaxation time of velocity, α and β are the fractional parameters of shear stress and shear strain, respectively, and $\partial^{\alpha} / \partial t^{\alpha}$ is the Caputo fractional derivative operator defined as [36]:

$$\frac{\partial^{\alpha}}{\partial t^{\alpha}} f(x,y,t) = \frac{1}{\Gamma(1-\alpha)} \int_0^t \frac{\partial f(x,y,\eta)}{\partial \eta} \frac{d\eta}{(t-\eta)^{\alpha}}, \tag{4}$$

where $\Gamma(\bullet)$ is the Gamma function.

For the considered problem, the derivative of ε on the right side of Eq (3) is interpreted as a fractional integral of order $\beta - 1$, and the constitutive relation becomes:

$$\tau_{xy} + \lambda_1^{\alpha} \frac{\partial^{\alpha} \tau_{xy}}{\partial t^{\alpha}} = G\lambda_1^{\beta} \frac{\partial^{\beta-1} \zeta}{\partial t^{\beta-1}} = \mu\lambda_1^{\beta-1} \frac{\partial^{\beta-1}}{\partial t^{\beta-1}} \left(\frac{\partial u}{\partial y} \right), \tag{5}$$

where μ is the dynamic viscosity that satisfies $\mu = \rho_f \nu_f$.

Combining Eqs (1) and (5), the momentum equation is transformed in the following form:

$$\begin{aligned} &\left(\lambda_1^{1-\beta} \frac{\partial^{1-\beta}}{\partial t^{1-\beta}} + \lambda_1^{1+\alpha-\beta} \frac{\partial^{1+\alpha-\beta}}{\partial t^{1+\alpha-\beta}} \right) \left(\frac{1}{\phi} \frac{\partial u}{\partial t} + \frac{1}{\phi^2} \left[\frac{\partial}{\partial x}(uu) + \frac{\partial}{\partial y}(vu) \right] \right) \\ &= \frac{\nu_f}{\phi} \frac{\partial^2 u}{\partial y^2} + \left(\lambda_1^{1-\beta} \frac{\partial^{1-\beta}}{\partial t^{1-\beta}} + \lambda_1^{1+\alpha-\beta} \frac{\partial^{1+\alpha-\beta}}{\partial t^{1+\alpha-\beta}} \right) \left[g\beta_T (T - T_{\infty}) - \frac{\nu_f}{K} u - \frac{c_F}{\sqrt{K}} u^2 \right] \end{aligned} \tag{6}$$

A similar process is conducted on heat flux using generalized Fourier's law with the double fractional Maxwell model; hence, Eq (2) is also transformed as follows:

$$\left(\lambda_2^{1-\eta} \frac{\partial^{1-\eta}}{\partial t^{1-\eta}} + \lambda_2^{1+\gamma-\eta} \frac{\partial^{1+\gamma-\eta}}{\partial t^{1+\gamma-\eta}} \right) \left[\sigma \frac{\partial T}{\partial t} + \frac{\partial}{\partial x}(uT) + \frac{\partial}{\partial y}(vT) \right] = \alpha_m \frac{\partial^2 T}{\partial y^2}, \tag{7}$$

where $\sigma=(\rho c)_m/(\rho c)_f$ is the thermal capacity ratio, $\alpha_m=k_m/(\rho c)_f$ is the thermal diffusivity, and k_m is the thermal conductivity of the porous medium. The fractional parameters of heat transfer have similar properties to Eq (3), namely λ_2, γ, and η.

The initial and boundary conditions are given as:

$$u(x,y,0)=0,\frac{\partial u(x,y,0)}{\partial t}=0,\ v(x,y,0)=0,T(x,y,0)=T_\infty,$$

$$\frac{\partial T(x,y,0)}{\partial t}=0,u(x,0,t)=0,\ v(x,0,t)=0,\ -k_m\frac{\partial T(x,0,t)}{\partial y}=q_w,$$

$$u(0,y,t)=0,\ T(0,y,t)=T_\infty,\ u(x,\infty,t)=0,\ T(x,\infty,t)=T_\infty.$$

The dimensionless variables are employed in the following form:

$$x^*=\frac{x}{L},\ y^*=\frac{y}{L}Ra^{1/4},\ u^*=\frac{uL}{\alpha_m}Ra^{-1/2},\ v^*=\frac{vL}{\alpha_m}Ra^{-1/4},\ t^*=\frac{\alpha_m t}{L^2}Ra^{1/2},\lambda_1{}^*=\frac{\alpha_m\lambda_1}{L^2}Ra^{1/2},$$

$$\lambda_2{}^*=\frac{\alpha_m\lambda_2}{L^2}Ra^{1/2},\ \theta=\frac{T-T_\infty}{L(q_w/k_m)},\ Pr=\frac{\nu_f}{\alpha_m},\ Ra=\frac{g\beta_T L^4 q_w}{\alpha_m\nu_f k_m},\ Da=\frac{K}{L^2},\ \Lambda=\frac{c_f\phi^2 L}{\sqrt{K}},$$

where L is the plate length, Pr is the Prandtl number, Ra is the Rayleigh number, Da is the Darcy number, and Λ is the inertial parameter that quantifies the nonlinear drag in porous media when flow velocity is high. This parameter is critical for modeling flows in oil/gas reservoirs, groundwater systems, and industrial porous materials.

Finally, the dimensionless governing equations are normalized by omitting the mark "*" for simplification as:

$$\frac{\partial u}{\partial x}+\frac{\partial v}{\partial y}=0, \tag{8}$$

$$\begin{aligned}&\left(\lambda_1{}^{1-\beta}\frac{\partial^{1-\beta}}{\partial t^{1-\beta}}+\lambda_1{}^{1+\alpha-\beta}\frac{\partial^{1+\alpha-\beta}}{\partial t^{1+\alpha-\beta}}\right)\left[\phi\frac{\partial u}{\partial t}+\frac{\partial}{\partial x}(uu)+\frac{\partial}{\partial y}(vu)\right]\\&=\phi Pr\frac{\partial^2 u}{\partial y^2}+\left(\lambda_1{}^{1-\beta}\frac{\partial^{1-\beta}}{\partial t^{1-\beta}}+\lambda_1{}^{1+\alpha-\beta}\frac{\partial^{1+\alpha-\beta}}{\partial t^{1+\alpha-\beta}}\right)\left(\phi^2 Pr\theta-\frac{\phi^2 Pr}{DaRa^{1/2}}u-\Lambda u^2\right),\end{aligned} \tag{9}$$

$$\left(\lambda_2^{1-\eta}\frac{\partial^{1-\eta}}{\partial t^{1-\eta}}+\lambda_2^{1+\gamma-\eta}\frac{\partial^{1+\gamma-\eta}}{\partial t^{1+\gamma-\eta}}\right)\left[\sigma\frac{\partial\theta}{\partial t}+\frac{\partial}{\partial x}(u\theta)+\frac{\partial}{\partial y}(v\theta)\right]=\frac{\partial^2\theta}{\partial y^2}. \tag{10}$$

The dimensionless initial and boundary conditions are derived as:

$$u(x,y,0)=0,\frac{\partial u(x,y,0)}{\partial t}=0,\ \ v(x,y,0)=0,\theta(x,y,0)=0,$$

$$\frac{\partial\theta(x,y,0)}{\partial t}=0,u(x,0,t)=0,\ \ v(x,0,t)=0,\ \ -\frac{\partial\theta(x,0,t)}{\partial y}=1,$$

$$u(0,y,t)=0,\ \ \theta(0,y,t)=0,\ \ u(x,\infty,t)=0,\ \ \theta(x,\infty,t)=0.$$

3. Numerical discretization method

In the following chapter, the fractional finite volume method is employed to discretize the governing equations. To obtain the integration of the governing equations over a single control volume, the solution region is discretized into a finite control volume, and the schematic diagram of the grid system, as shown in Figure 1, is established, where the central nodal point is noted by P. Then, we integrate Eq (10) over a control volume and finite time step Δt. Finally, a numerical discrete iterative equation is yielded by the following approximation steps.

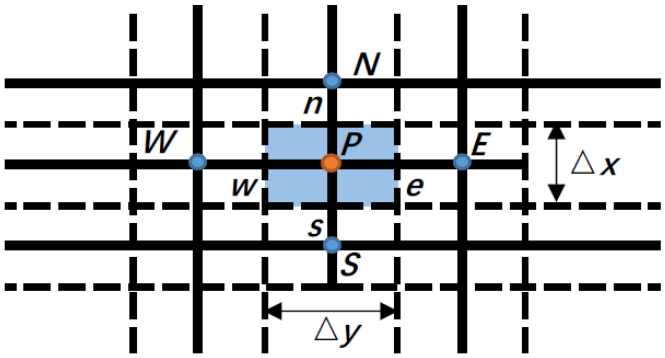

Figure 1. Schematic diagram of the grid system for the control volume.

The first term with time derivative in Eq (10) is discretized using the backward difference scheme, which yields:

$$\int_t^{t+\Delta t}\int_{\Delta V}\sigma\frac{\partial\theta}{\partial t}dVdt=\sigma\left(\theta_P^k-\theta_P^{k-1}\right)\cdot\Delta V+O(\Delta t),\tag{11}$$

where $\Delta V=\Delta x\cdot\Delta y$ is the control volume.

The volume integral of convective term is transformed into a surface integral form that is estimated by the first-order upwind difference formula as follows:

$$\int_t^{t+\Delta t}\int_{\Delta V}\frac{\partial}{\partial x}(u\theta)dVdt=\left[\left(uA\theta\right)_n^k-\left(uA\theta\right)_s^k\right]\cdot\Delta t=\left(u_P^{k-1}A_n\theta_P^k-u_S^{k-1}A_s\theta_S^k\right)\cdot\Delta t++O(\Delta x),\tag{12}$$

$$\int_t^{t+\Delta t}\int_{\Delta V}\frac{\partial}{\partial y}(v\theta)dVdt=\left[\left(vA\theta\right)_e^k-\left(vA\theta\right)_w^k\right]\cdot\Delta t=\left(v_E^{k-1}A_e\theta_E^k-v_P^{k-1}A_w\theta_P^k\right)\cdot\Delta t+O(\Delta y),\tag{13}$$

where A represents the face area, $A_w=A_e=\Delta x$, $A_n=A_s=\Delta y$.

The right side of Eq (10), representing the term of the diffusion effect, is approximated by a central difference format for the interface gradient:

$$\int_t^{t+\Delta t}\int_{\Delta V}\frac{\partial^2\theta}{\partial y^2}dVdt=\left[\left(A\frac{\partial\theta}{\partial y}\right)_e^k-\left(A\frac{\partial\theta}{\partial y}\right)_w^k\right]\cdot\Delta t=\left(A_e\frac{\theta_E^k-\theta_P^k}{\Delta y}-A_w\frac{\theta_P^k-\theta_W^k}{\Delta y}\right)\cdot\Delta t+O(\Delta y^2).\tag{14}$$

The fractional derivative of time is approximated discretely by the fractional $L1$ numerical method [37]:

$$\frac{\partial^\omega}{\partial t^\omega}f(t_k)=\frac{\Delta t^{-\omega}}{\Gamma(2-\omega)}\left[f(t_k)-\omega_{k-1}f(t_0)-\sum_{j=1}^{k-1}\left(\omega_{j-1}-\omega_j\right)f(t_{k-j})\right]+O\left(\Delta t^{2-\omega}\right),\tag{15}$$

where $0<\omega<1$, $\omega_j=(j+1)^{1-\omega}-j^{1-\omega}$, $\omega=1-\beta$ or $\omega=1+\alpha-\beta$.

Hence, the integrations of the multi-term fractional derivatives in Eq (10) yield:

$$\begin{aligned}&\int_t^{t+\Delta t}\int_{\Delta V}\lambda^\omega\frac{\partial^\omega}{\partial t^\omega}\left(\frac{\partial\theta}{\partial t}\right)dVdt\\&=\frac{\lambda^\omega\cdot\Delta t^{-\omega}\cdot\Delta V}{\Gamma(2-\omega)}\left[\theta_P^k-\theta_P^{k-1}-\sum_{j=1}^{k-1}\left(\omega_{j-1}-\omega_j\right)\left(\theta_P^{k-j}-\theta_P^{k-j-1}\right)\right]+R_1,\end{aligned}\tag{16}$$

$$\begin{aligned}&\int_t^{t+\Delta t}\int_{\Delta V}\lambda^\omega\frac{\partial^\omega}{\partial t^\omega}\frac{\partial}{\partial x}(u\theta)\,dVdt\\&=\frac{\lambda^\omega\cdot\Delta t^{-\omega+1}}{\Gamma(2-\omega)}\left[u_P^{k-1}A_n\theta_P^k-u_S^{k-1}A_s\theta_S^k-\sum_{j=1}^{k-1}\left(\omega_{j-1}-\omega_j\right)\left(u_P^{k-j-1}A_n\theta_P^{k-j}-u_S^{k-j-1}A_s\theta_S^{k-j}\right)\right]+R_2,\end{aligned}\tag{17}$$

$$\begin{aligned}&\int_t^{t+\Delta t}\int_{\Delta V}\lambda^\omega\frac{\partial^\omega}{\partial t^\omega}\frac{\partial}{\partial y}(v\theta)\,dVdt\\&=\frac{\lambda^\omega\cdot\Delta t^{-\omega+1}}{\Gamma(2-\omega)}\left[v_E^{k-1}A_e\theta_E^k-v_P^{k-1}A_w\theta_P^k-\sum_{j=1}^{k-1}\left(\omega_{j-1}-\omega_j\right)\left(v_E^{k-j-1}A_e\theta_E^{k-j}-v_P^{k-j-1}A_w\theta_P^{k-j}\right)\right]+R_3,\end{aligned}\tag{18}$$

where the truncation errors $R_1\le C(\Delta t)$, $R_2\le C(\Delta t+\Delta x)$, $R_3\le C(\Delta t+\Delta y)$.

The integer-order derivatives of the momentum equation are dealt with in a similar process. The single term θ or u in Eq (9) is integrated by a semi-implicit scheme as:

$$\int_t^{t+\Delta t}\int_{\Delta V}\theta\,dVdt=\frac{\Delta V\Delta t}{2}\cdot\left(\theta_P^k+\theta_P^{k-1}\right)+O(\Delta t),\tag{19}$$

$$\int_t^{t+\Delta t}\int_{\Delta V}\lambda^{\omega}\frac{\partial^{\omega}}{\partial t^{\omega}}\theta\, dVdt=\frac{\lambda^{\omega}\cdot\Delta t^{-\omega+1}\cdot\Delta V}{2\Gamma(2-\omega)}\bullet\left[\theta_P^k+\theta_P^{k-1}-\sum_{j=1}^{k-1}\left(\omega_{j-1}-\omega_j\right)\left(\theta_P^{k-j}+\theta_P^{k-j-1}\right)\right]+O(\Delta t)\cdot \tag{20}$$

Particularly, the non-Darcy term in Eq (9) is integrated using linear treatment:

$$\int_t^{t+\Delta t}\int_{\Delta V}\Lambda u^2\, dVdt=\Lambda\Delta V\Delta t\cdot u_P^{k-1}u_P^k++O\left(\Delta t+\Delta x+\Delta y\right). \tag{21}$$

Finally, the iterative calculation formula on the node P is derived:

$$a_P\phi_P^k=a_S\phi_S^k+a_W\phi_W^k+a_E\phi_E^k+S_P+\psi, \tag{22}$$

where ϕ denotes velocity or temperature, and ψ is the truncation error that satisfies $\psi\le C\left(\Delta x+\Delta y+\Delta t\right)$. For the temperature term, the coefficients of Eq (22) are in the following forms:

$$a_P=R\cdot\left(\frac{\sigma\Delta V}{\Delta t}+\Delta y\cdot u_P^{k-1}-\Delta x\cdot v_P^{k-1}\right)+\frac{2\Delta x}{\Delta y},\quad R=\frac{\lambda^{1-\beta}\cdot\Delta t^{\beta-1}}{\Gamma\left(1+\beta\right)}+\frac{\lambda^{1+\alpha-\beta}\cdot\Delta t^{\beta-\alpha-1}}{\Gamma\left(1+\beta-\alpha\right)},$$

$$a_S=R\cdot\Delta y\cdot u_S^{k-1},\quad a_w=\frac{\Delta x}{\Delta y},\quad a_E=\frac{\Delta x}{\Delta y}-R\cdot\Delta x\cdot v_E^{k-1},$$

$$\begin{aligned}S_P&=R\cdot\frac{\sigma\Delta V}{\Delta t}\cdot\theta_P^{k-1}+\frac{\Delta V}{\Delta t}\cdot\sum_{j=1}^{k-1}\chi_j\left(\theta_P^{k-j}-\theta_P^{k-j-1}\right)\\&+\Delta y\cdot\sum_{j=1}^{k-1}\chi_j\left(u_P^{k-j-1}\theta_P^{k-j}-u_S^{k-j-1}\theta_S^{k-j}\right)+\Delta x\cdot\sum_{j=1}^{k-1}\chi_j\left(v_E^{k-j-1}\theta_E^{k-j}-v_P^{k-j-1}\theta_P^{k-j}\right),\end{aligned}$$

$$\chi_j=\frac{\lambda^{1-\beta}\cdot\Delta t^{\beta-1}}{\Gamma\left(1+\beta\right)}\cdot\left[2j^{\beta}-\left(j+1\right)^{\beta}-\left(j-1\right)^{\beta}\right]+\frac{\lambda^{1+\alpha-\beta}\cdot\Delta t^{\beta-\alpha-1}}{\Gamma\left(1+\beta-\alpha\right)}\cdot\left[2j^{\beta-\alpha}-\left(j+1\right)^{\beta-\alpha}-\left(j-1\right)^{\beta-\alpha}\right]\cdot$$

Additionally, the expression of the velocity component in y-direction is obtained by the integral continuity equation:

$$\begin{aligned}&\int_t^{t+\Delta t}\int_{\Delta V}\frac{\partial u}{\partial x}\, dVdt+\int_t^{t+\Delta t}\int_{\Delta V}\frac{\partial v}{\partial y}\, dVdt=\frac{\Delta t}{2}\left[\left(uA\right)_n^k-\left(uA\right)_s^k+\left(uA\right)_n^{k-1}-\left(uA\right)_s^{k-1}\right]\\&+\frac{\Delta t}{2}\left[\left(vA\right)_e^k-\left(vA\right)_w^k+\left(vA\right)_e^{k-1}-\left(vA\right)_w^{k-1}\right]=0,\end{aligned} \tag{23}$$

$$v_P^k=-v_P^{k-1}+v_W^k+v_W^{k-1}-\frac{\Delta y}{\Delta x}\left(u_P^k-u_S^k+u_P^{k-1}-u_S^{k-1}\right)+O\left(\Delta x+\Delta y\right). \tag{24}$$

4. Validation of the numerical results

The numerical values ϕ^k at the kth time level are derived from the iteration equations. The coefficient matrix in each solving step is tri-diagonal and full-rank; therefore, the fractional difference scheme is uniquely solvable. To validate the numerical accuracy of the fractional difference scheme, two source terms in the special case are introduced as:

$$\frac{\partial u}{\partial x}+\frac{\partial v}{\partial y}=0\,, \tag{25}$$

$$\begin{aligned}&\left(\lambda_1^{1-\beta}\frac{\partial^{1-\beta}}{\partial t^{1-\beta}}+\lambda_1^{1+\alpha-\beta}\frac{\partial^{1+\alpha-\beta}}{\partial t^{1+\alpha-\beta}}\right)\left(\phi\frac{\partial u}{\partial t}+\frac{\partial}{\partial x}(uu)+\frac{\partial}{\partial y}(vu)\right)=\phi Pr\frac{\partial^2 u}{\partial y^2}\\&+\left(\lambda_1^{1-\beta}\frac{\partial^{1-\beta}}{\partial t^{1-\beta}}+\lambda_1^{1+\alpha-\beta}\frac{\partial^{1+\alpha-\beta}}{\partial t^{1+\alpha-\beta}}\right)\left[\phi^2 Pr\theta-\frac{\phi^2 Pr}{DaRa^{1/2}}u-\Lambda u^2\right]+f_1(x,y,t)\end{aligned}\,, \tag{26}$$

$$\left(\lambda_2^{1-\eta}\frac{\partial^{1-\eta}}{\partial t^{1-\eta}}+\lambda_2^{1+\gamma-\eta}\frac{\partial^{1+\gamma-\eta}}{\partial t^{1+\gamma-\eta}}\right)\left[\sigma\frac{\partial\theta}{\partial t}+\frac{\partial}{\partial x}(u\theta)+\frac{\partial}{\partial y}(v\theta)\right]=\frac{\partial^2\theta}{\partial y^2}+f_2(x,y,t)\,. \tag{27}$$

The initial conditions and boundary conditions are reduced to homogeneous forms:

$$u(x,y,0)=0\,,\frac{\partial u(x,y,0)}{\partial t}=0\,,\ \ v(x,y,0)=0\,,\theta(x,y,0)=0\,,$$

$$\frac{\partial\theta(x,y,0)}{\partial t}=0\,,u(x,0,t)=0\,,\ \ v(x,0,t)=0\,,\theta(x,0,t)=0\,,$$

$$u(0,y,t)=0\,,\ \ \theta(0,y,t)=0\,,\ \ u(x,\infty,t)=0\,,\ \ \theta(x,\infty,t)=0\,.$$

Let

$$\begin{aligned}&f_1(x,y,t)=-2\phi Prx^2(1-x)^2\left(1-6y+6y^2\right)t^2+2\phi x^2(1-x)^2y^2(1-y)^2\\&\times\left\{\frac{\lambda_1^{1-\beta}t^{\beta}}{\Gamma(1+\beta)}+\frac{\lambda_1^{1+\alpha-\beta}t^{\beta-\alpha}}{\Gamma(1+\beta-\alpha)}-\left(\phi Pr-\frac{\phi Pr}{DaRa^{1/2}}\right)\times\left[\frac{\lambda_1^{1-\beta}t^{1+\beta}}{\Gamma(2+\beta)}+\frac{\lambda_1^{1+\alpha-\beta}t^{1+\beta-\alpha}}{\Gamma(2+\beta-\alpha)}\right]\right\}\\&+\left[\frac{24\lambda_1^{1-\beta}t^{3+\beta}}{\Gamma(4+\beta)}+\frac{24\lambda_1^{1+\alpha-\beta}t^{3+\beta-\alpha}}{\Gamma(4+\beta-\alpha)}\right]\times[2x^3(1-x)^3(1-2x)y^4(1-y)^4\\&-4x^3(1-x)^3(1-2x)y(1-y)(1-2y)\left(\frac{1}{3}y^3-\frac{1}{2}y^4+\frac{1}{5}y^5\right)+\Lambda x^4(1-x)^4y^4(1-y)^4\Big],\end{aligned}$$

$$f_2(x,y,t) = -2x^2(1-x)^2(1-6y+6y^2)t^2$$
$$+\left[\frac{\lambda_2^{1-\eta}t^{\eta}}{\Gamma(1+\eta)}+\frac{\lambda_2^{1+\gamma-\eta}t^{\eta-\gamma}}{\Gamma(1+\eta-\gamma)}\right]\times 2\sigma x^2(1-x)^2y^2(1-y)^2$$
$$+\left[\frac{24\lambda_2^{1-\eta}t^{3+\eta}}{\Gamma(4+\eta)}+\frac{24\lambda_2^{1+\gamma-\eta}t^{3+\eta-\gamma}}{\Gamma(4+\eta-\gamma)}\right]\times\left[2x^3(1-x)^3(1-2x)y^4(1-y)^4\right.$$
$$\left.-4x^3(1-x)^3(1-2x)y(1-y)(1-2y)\left(\frac{1}{3}y^3-\frac{1}{2}y^4+\frac{1}{5}y^5\right)\right].$$

The exact solutions of Eqs (25)–(27) are constructed in the following forms:

$$u(x,y,t) = x^2(1-x)^2y^2(1-y)^2t^2,$$

$$v(x,y,t) = -2x(1-x)(1-2x)\left(\frac{1}{3}y^3-\frac{1}{2}y^4+\frac{1}{5}y^5\right)t^2,$$

$$\theta(x,y,t) = x^2(1-x)^2y^2(1-y)^2t^2.$$

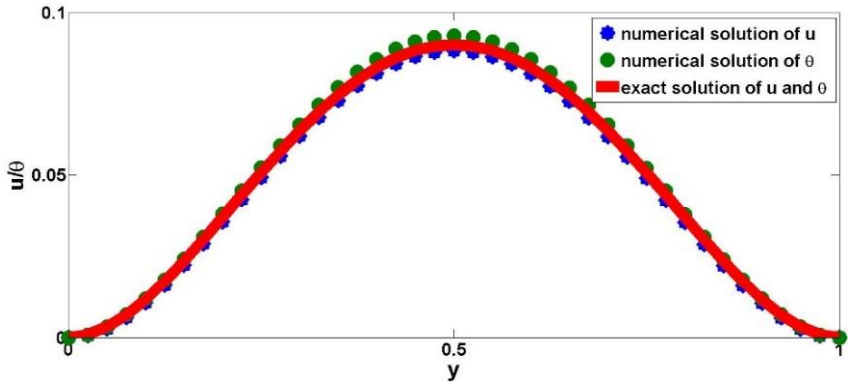

Figure 2. The comparison result of numerical solutions and analytical solutions.

Due to the strong nonlinearity and coupling of the control equation system, the constructed finite volume scheme is conditionally stable. Figure 2 describes the comparative analysis of numerical results and analytical solutions of velocity or temperature. The distributions maintain good agreement, and the truncation accuracy and convergence of the presented difference scheme are demonstrated accordingly.

5. Results and discussion

The effects of major parameters on fluid velocity distribution and the temperature gradient are analyzed, namely the fractional derivative parameters, Darcy number, porosity, and the inertial

parameter. For simplicity, other parameters are fixed as a constant, such as λ_1 and λ_2, which are both 0.1, Pr is 2, Ra is 10^6, and σ is 1.

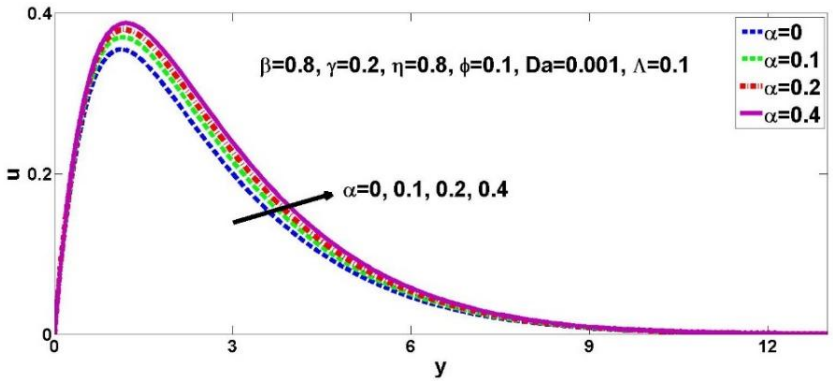

Figure 3. Influence of α on velocity profiles.

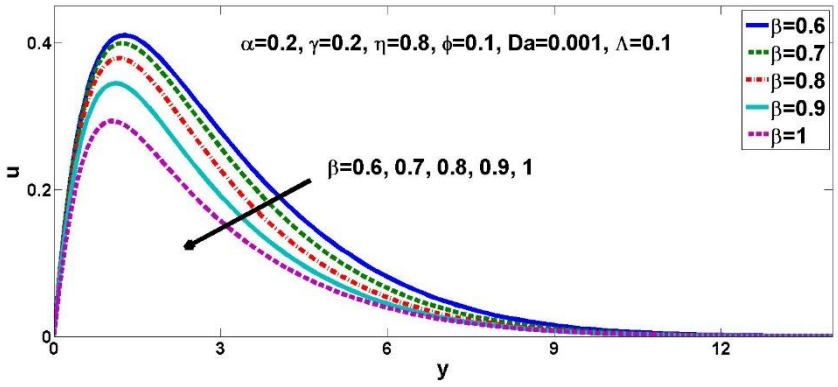

Figure 4. Influence of β on velocity profiles.

Figure 3 describes the variation characteristics of fluid velocity profiles with different α. With the augmentation of α, the velocity profile rises slightly, so that the variations are not sensitive, and the momentum boundary layer is almost unchanged. As $\alpha = 0$, the fluid transforms to fractional second-order fluid and has the smallest velocity. Figure 4 depicts the influence of β on velocity profiles. Oppositely, the velocity profile declines with the expansion of fractional shear strain parameter β. Thus, the extreme point of each profile moves closer to the plate. As $\beta = 1$, the fluid degrades into the single fractional Maxwell model but possesses the biggest value of velocity. These results demonstrate that the fractional shear strain parameter β has a greater influence on the velocity field. Figure 5 depicts the influence of β on temperature profiles. As β increases, the temperature distribution rises, but the thickness of the thermal boundary layer also has a slight augmentation.

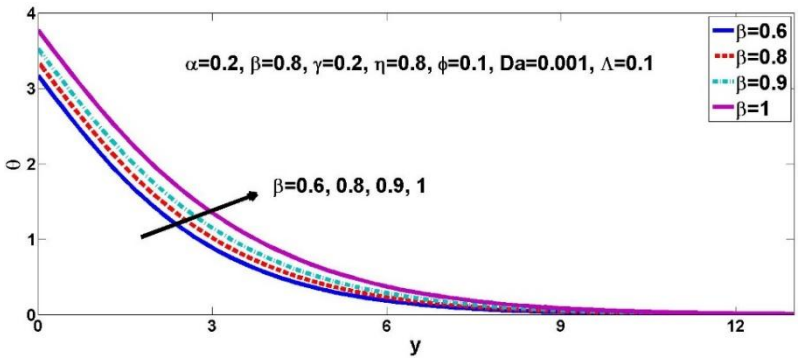

Figure 5. Influence of β on temperature profiles.

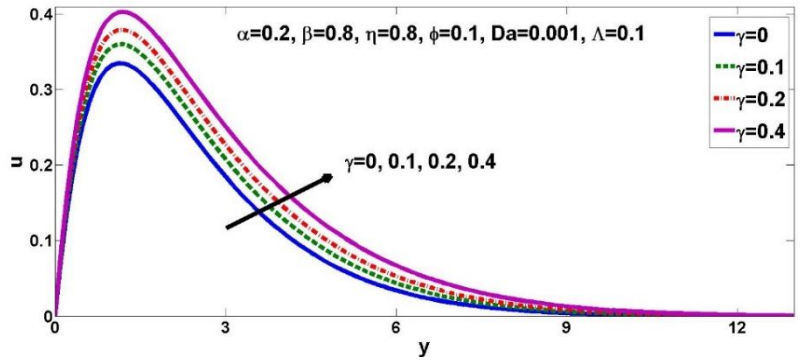

Figure 6. Influence of γ on velocity profiles.

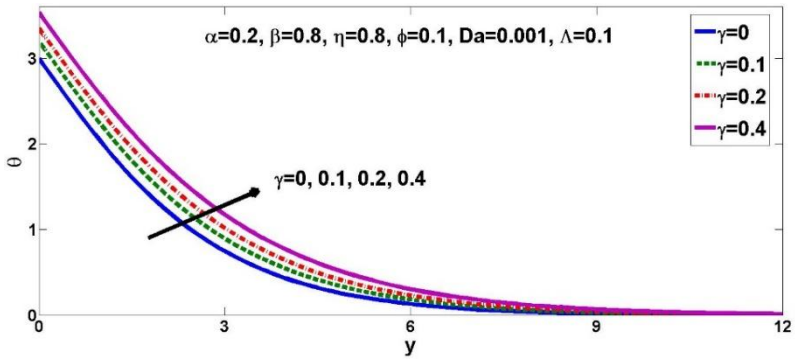

Figure 7. Influence of γ on temperature profiles.

The influence of γ on the velocity and temperature profiles are shown in Figures 6 and 7, respectively. With the increase of γ, the velocity and temperature profiles rise, and the field boundary layers become thicker with an increase in energy dissipation. As $\gamma = 0$, the fractional second order fluid has the lowest velocity and temperature profiles but maintains the highest transport efficiency. Distribution curves of fluid velocity and temperature for different η are illustrated in Figures 8 and 9,

respectively. With the augmentation of η, the velocity and temperature profiles decline remarkably, while the thickness of the momentum boundary layer and the thermal boundary layer becomes thinner. As $\eta = 1$, the single fractional Maxwell fluid has the lowest values of velocity and temperature, but the transfer efficiency remains the highest.

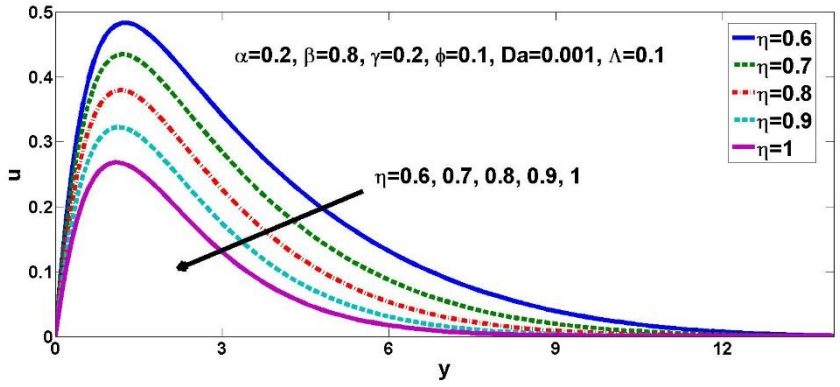

Figure 8. Influence of η on velocity profiles.

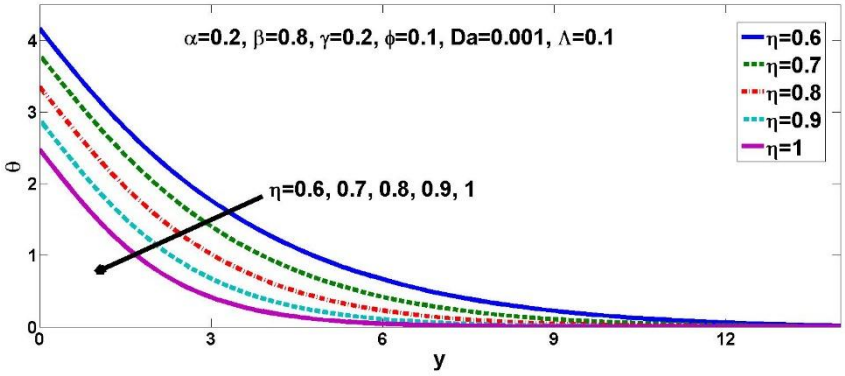

Figure 9. Influence of η on temperature profiles.

Figure 10 illustrates the influence of *Da* on velocity distributions. With the rise of the Darcy number, the velocity profile increases significantly first but intersects with each other as the distance from the plate increases. The gap between the curves decreases, which demonstrates that the sensitivity to Darcy number decreases. Figure 11 describes the velocity profiles for different ϕ. The increase in porosity results in a significant increase in fluid velocity distribution, and the extreme value of each profile moves further away from the plate, but the momentum boundary layer thickness remains unchanged. The temperature distribution curves for different ϕ are shown in Figure 12. With the augmentation of ϕ, the temperature gradient decreases significantly, and the thickness of the thermal boundary layer decreases. The gap between the curves decreases gradually, and the thermal sensitivity to porosity also decreases.

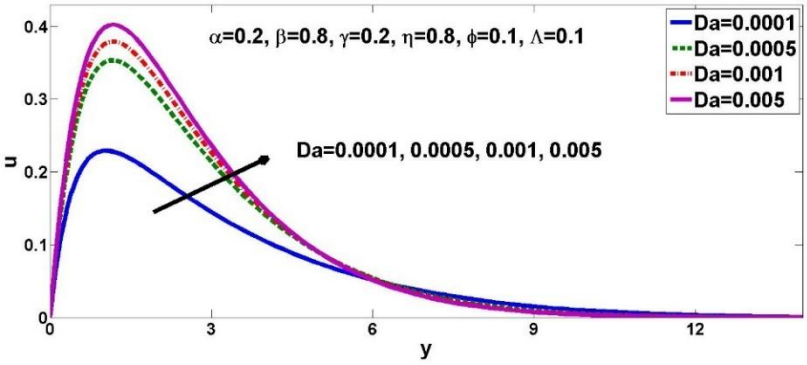

Figure 10. Influence of *Da* on velocity profiles.

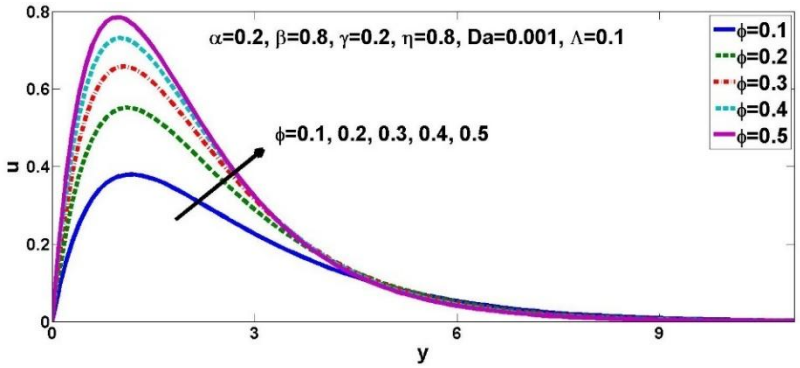

Figure 11. Influence of ϕ on velocity profiles.

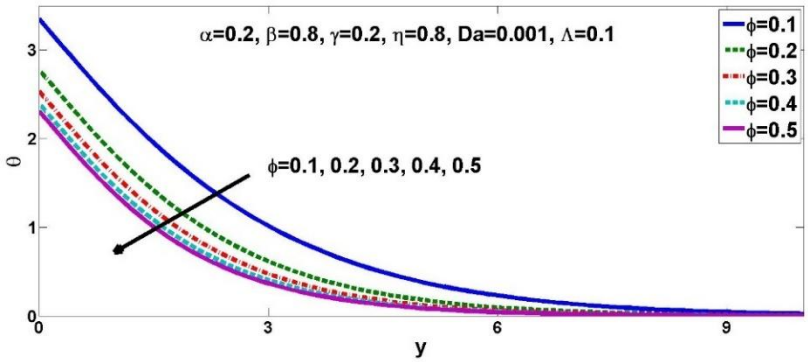

Figure 12. Influence of ϕ on temperature profiles.

The influence of Λ on velocity profiles is depicted in Figure 13. With the increase of Λ, the velocity profile first declines, intersects with others in the middle of the boundary layer, but rises slightly in the end. The temperature gradient distributions for different inertial parameters are illustrated in Figure 14. As the inertial parameter increases, the temperature distribution increases regularly, and the thickness of the thermal boundary layer enlarges slightly.

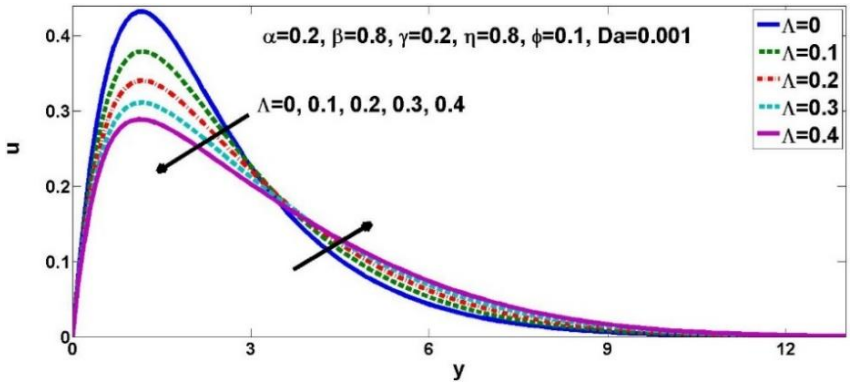

Figure 13. Influence of Λ on velocity profiles.

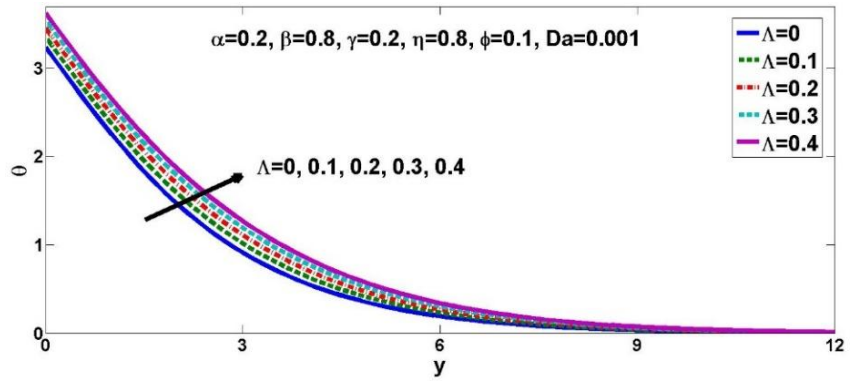

Figure 14. Influence of Λ on temperature profiles.

6. Conclusions

We investigated the unsteady natural convective heat transfer of a viscoelastic fluid in non-Darcy porous media. The double fractional Maxwell model combined with the generalized Fourier heat conduction theory is applied. The finite volume method combined with the $L1$ scheme of fractional derivatives was presented to solve the interrelated nonlinear equations. The influences of involved parameters on the velocity and temperature fields are analyzed in detail. The conclusion is summarized as follows: (i) The velocity rises with the increase of α, but declines with the augmentation of β. The temperature profile increases as β rises; (ii) distribution curves of fluid velocity and temperature rise with the increase of γ, but decline remarkably with the augmentation of η; (iii) with the rise of the Da, the velocity distribution increases significantly at first, but intersects with others. As ϕ increases, the velocity profile increases, but the temperature profile declines; (iv) as Λ rises, the velocity profile first declines and rises slightly in the end, while the temperature profiles increase regularly.

In the future, researchers could explore other fractional rheological models and employ high-order discretization techniques to improve computational efficiency for multi-scale fractional problems.

Use of AI tools declaration

The authors declare they have not used Artificial Intelligence (AI) tools in the creation of this article.

Acknowledgments

The work is supported by the Outstanding Youth Research Project of Anhui Universities (2023AH030075), National Natural Science Foundations of China (No. 12102093).

Conflict of interest

The authors declare there is no conflict of interest.

References

1. D. A. Nield, A. Bejan, *Convection in Porous Media*, 4th Edition, Springer-Verlag, New-York, 2013.
2. K. Vafai, C. L. Tien, Boundary and inertia effects on flow and heat transfer in porous media, *Int. J. Heat Mass Transfer*, **24** (1981), 195–203. https://doi.org/10.1016/0017-9310(81)90027-2
3. M. F. El-Amin, Double dispersion effects on natural convection heat and mass transfer in non-Darcy porous medium, *Appl. Math. Comput.*, **156** (2004), 1–17. https://doi.org/10.1016/j.amc.2003.07.001
4. P. Narayana, P. Murthy, Free convective heat and mass transfer in a doubly stratified non-darcy porous medium, *J. Heat Transfer*, **128** (2006), 1204–1212. https://doi.org/10.1115/1.2352788
5. D. Pal, H. Mondal, Effect of variable viscosity on MHD non-Darcy mixed convective heat transfer over a stretching sheet embedded in a porous medium with non-uniform heat source/sink, *Commun. Nonlinear Sci. Numer. Simul.*, **15** (2010), 1553–1564. https://doi.org/10.1016/j.cnsns.2009.07.002
6. A. A. El-Zehairy, M. M. Nezhad, V. Joekar-Niasar, I. Guymer, N. Kourra, M. A. Williams, Pore-network modelling of non-Darcy flow through heterogeneous porous media, *Adv. Water Resour.*, **131** (2019), 103378. https://doi.org/10.1016/j.advwatres.2019.103378
7. D. Y. Song, X. F. Song, T. Q. Jiang, Study of rheological characterization of Fenugreek gum with modified Maxwell model, *Chin. J. Chem. Eng.*, **8** (2000), 85–88.
8. Z. Xu, W. Chen, A fractional-order model on new experiments of linear viscoelastic creep of Hami Melon, *Comput. Math. Appl.*, **66** (2013), 677–681.https://doi.org/10.1016/ j.camwa.2013.01.033
9. X. Yang, X. Jiang, J. Kang, Parameter identification for fractional fractal diffusion model based on experimental data, *Chaos*, **29** (2019), 083134. https://doi.org/10.1063/1.5111832
10. D. G. Yao, A fractional dashpot for nonlinear viscoelastic fluids, *J. Rheol.*, **62** (2018), 619–629. https://doi.org/10.1122/1.5012504
11. X. L. Su, W. X. Xu, W. Chen, H. X. Yang, Fractional creep and relaxation models of viscoelastic materials via a non-Newtonian time-varying viscosity: Physical interpretation, *Mech. Mater.*, **140** (2020), 103222. https://doi.org/10.1016/j.mechmat.2019.103222

12. W. Tan, W. Pan, M. Xu, A note on unsteady flows of a viscoelastic fluid with the fractional Maxwell model between two parallel plates, *Int. J. Non-Linear Mech.*, **38** (2003), 645–650. https://doi.org/10.1016/S0020-7462(01)00121-4
13. L. Wei, Y. F. Yang, Optimal order finite difference/local discontinuous Galerkin method for variable-order time-fractional diffusion equation, *J. Comput. Appl. Math.*, **383** (2021), 113129. https://doi.org/10.1016/j.cam.2020.113129
14. Y. L. Feng, X. D. Zhang, Y. Chen, L. Wei, A compact finite difference scheme for solving fractional Black-Scholes option pricing model, *J. Inequal. Appl.*, **2025** (2025), 36. https://doi.org/10.1186/s13660-025-03261-2
15. X. D. Zhang, L. Wei, J. Liu, Application of the LDG method using generalized alternating numerical flux to the fourth-order time-fractional sub-diffusion model, *Appl. Math. Lett.*, **168** (2025), 109580. https://doi.org/10.1016/j.aml.2025.109580
16. K. J. Wang, H. W. Zhu, S. Li, F. Shi, G. Li, X. L. Liu, Bifurcation analysis, chaotic behaviors, variational principle, Hamiltonian and diverse optical solitons of the fractional complex Ginzburg–Landau model, *Int. J. Theor. Phys.*, **64** (2025), 134. https://doi.org/10.1007/s10773-025-05977-9
17. K. J. Wang, An effective computational approach to the local fractional low-pass electrical transmission lines model, *Alexandria Eng. J.*, **110** (2025), 629–635. https://doi.org/10.1016/j.aej.2024.07.021
18. K. J. Wang, M. Li, Variational principle of the unstable nonlinear Schrödinger equation with fractal derivatives, *Axioms*, **14** (2025), 376. https://doi.org/10.3390/axioms14050376
19. T. Hayat, S. Nadeem, S. Asghar, Periodic unidirectional flows of a viscoelastic fluid with the fractional Maxwell model, *Appl. Math. Comput.*, **151** (2004), 153–161. https://doi.org/10.1016/S0096-3003(03)00329-1
20. Y. Yin, K. Zhu, Oscillating flow of a viscoelastic fluid in a pipe with the fractional Maxwell model, *Appl. Math. Comput.*, **173** (2006), 231–242. https://doi.org/10.1016/j.amc.2005.04.001
21. X. H. Chen, W. D. Yang, X. R. Zhang, F. W. Liu, Unsteady boundary layer flow of viscoelastic MHD fluid with a double fractional Maxwell model, *Appl. Math. Lett.*, **95** (2019), 143–149. https://doi.org/10.1016/j.aml.2019.03.036
22. W. D. Yang, X. H. Chen, X. R. Zhang, L. C. Zheng, F. W. Liu, Flow and heat transfer of double fractional Maxwell fluids over a stretching sheet with variable thickness, *Appl. Math. Modell.*, **80** (2020), 204–216. https://doi.org/10.1016/j.apm.2019.11.017
23. W. D. Yang, J. W. Zhao, X. H. Chen, K. Fang, Z. Y. Jiang, Z. Lin, et al., Aortic aneurysm hemodynamics based on a double fractional Maxwell arterial model, *Phys. Fluids*, **37** (2025), 013117. https://doi.org/10.1063/5.0246815
24. M. Caputo, W. Plastino, Diffusion in porous layers with memory, *Geophys. J. Int*., **158** (2004), 385–396. https://doi.org/10.1111/j.1365-246x.2004.02290.x
25. M. Hashan, L. N. Jahan, T. Zaman, S. Imtiaz, M. E. Hossain, Modelling of fluid flow through porous media using memory approach: A review, *Math. Comput. Simul*., **177** (2020), 643–673. https://doi.org/10.1016/j.matcom.2020.05.026
26. H.W. Zhou, S. Yang, Fractional derivative approach to non-Darcian flow in porous media, *J. Hydrol*., **566** (2018), 910–918. https://doi.org/10.1016/j.jhydrol.2018.09.039

27. H. W. Zhou, S. Yang, S. Q. Zhang, Modeling non-Darcian flow and solute transport in porous media with the Caputo-Fabrizio derivative, *Appl. Math. Modell.*, **68** (2019), 603–615. https://doi.org/10.1016/j.apm.2018.09.042
28. S. Yang, L. P. Wang, S. Q. Zhang, Conformable derivative: Application to non-Darcian flow in low-permeability porous media, *Appl. Math. Lett.*, **79** (2017), 105–110. https://doi.org/10.1016/j.aml.2017.12.006
29. G. Alaimo, V. Piccolo, A. Cutolo, L. Deseri, M. Fraldi, M. Zingales, A fractional order theory of poroelasticity, *Mech. Res. Commun.*, **100** (2019), 103395. https://doi.org/10.1016/j.mechrescom.2019.103395
30. Q. Wei, H. W. Zhou, S. Yang, Non-Darcy flow models in porous media via Atangana-Baleanu derivative, *Chaos Solitons Fractals*, **141** (2020), 110335. https://doi.org/10.1016/j.chaos.2020.110335
31. K. J. Wang, F. Shi, A new fractal model of the convective-radiative fins with temperature-dependent thermal conductivity, *Therm. Sci.*, **27** (2023), 2831–2837. https://doi.org/10.2298/TSCI220917207W
32. K. J. Wang, Variational approach for the fractional exothermic reactions model with constant heat source in porous medium, *Therm. Sci.*, **27** (2023), 2879–2885. https://doi.org/10.2298/TSCI220922211W
33. D. Parmar, S. Murthy, B. Kumar, S. Kumar, Numerical simulation of fractional order double diffusive convective nanofluid flow in a wavy porous enclosure, *Int. J. Heat Fluid Flow*, **112** (2025), 109749. https://doi.org/10.1016/j.ijheatfluidflow.2025.109749
34. A. Haider, M. S. Anwar, Y. F. Nie, T. Muhammad, Numerical simulations of heat and mass transfer in Sutterby fluid within porous media using Caputo fractional derivative, *Int. Commun. Heat Mass Transfer*, **164** (2025), 108850. https://doi.org/10.1016/j.icheatmasstransfer.2025.108850
35. C. Friedrich, Relaxation and retardation functions of the Maxwell model with fractional derivatives, *Rheol. Acta*, **30** (1991), 151–158.
36. I. Podlubny, *Fractional Differential Equations*, Academic Press, San Diego, (1999), 78–85.
37. F. Liu, P. Zhuang, V. Anh, I. Turner, K. Burrage, Stability and convergence of the difference methods for the space time fractional advection diffusion equation, *Appl. Math. Comput.*, **191** (2007), 12–20. https://doi.org/10.1016/j.amc.2006.08.162

AIMS Press